Available online at www.sciencedirect.com
ScienceDirect
Ceramics International 38 (2012) 23–28
CERAMICS INTERNATIONAL
www.elsevier.com/locate/ceramint

Transparent yttria stabilized zirconia from glycine-nitrate process by spark plasma sintering

Liwen Lei [a,b,*], Zhengyi Fu [a], Hao Wang [a], Soo Wohn Lee [c], Koichi Niihara [d]

[a] State Key Lab of Advanced Technology for Materials Synthesis and Processing, Wuhan University of Technology, Wuhan 430070, China
[b] School of Materials Science and Engineering, Wuhan University of Technology, Wuhan 430070, China
[c] Department of Environmental Engineering, Sun Moon University, Chungnam 336-708, Republic of Korea
[d] Extreme Energy-Density Research Institute, Nagaoka University of Technology, 1603-1 Kamitomioka, Nagaoka, Niigata 940-2188, Japan

Received 30 March 2011; received in revised form 18 May 2011; accepted 23 May 2011
Available online 27th May 2011

Abstract

Nanosized cubic yttria-stabilized zirconia (ZrO_2–8 mol% Y_2O_3) powder was synthesized via a glycine-nitrate process combining with high-energy ball milling. Effect of the calcination temperature on the sintering activity of the powders was discussed. The present investigations demonstrated the most favorable calcination temperature was 900 °C for obtaining fine nanopowders with high sinterability. Consolidation of the nanopowder was carried out by spark plasma sintering at 1200–1350 °C for 5 min. Transparent ceramics fabricated could be achieved at 1300 °C. Optical transmittance calculation based on Mie theory fits well with the experimental results of the transparent specimen sintered at 1300 °C, while the inconsistence for the specimen sintered at 1350 °C above 600 nm might be attributed to the scattering by grain boundaries and higher oxygen vacancy content.

Keywords: Glycine-nitrate process; Ball milling; Spark plasma sintering; Optical transmission; Zirconia ceramics

1. Introduction

Zirconia has been widely used because of their exceptional mechanical and functional properties, such as high hardness, toughness, high oxygen diffusivity and low thermal conductivity. Yttria addition assures zirconia stabilization in the cubic structure at high temperature and also provides oxygen vacancies. This improves ionic conductivity and makes stabilized ZrO_2 appropriate for use an electrolyte in solid oxide fuel cells. Recently there has been increasing interest in transparent cubic yttria-stabilized zirconia (ZrO_2–8 mol% Y_2O_3, 8YSZ) ceramics because of its unique optical properties. The cubic zirconia has a refractive index of 2.2, which has never been attained in optical glasses and is higher than other oxides [1,2]. Polycrystalline 8YSZ ceramics are highly expected to serve as a multifunctional material in optical applications provided it can combine transparency with excellent mechanical/thermal properties [3].

In recent years, a number of different techniques have been developed to fabricate YSZ nanopowder, such as sol–gel [5,6], hydrothermal treatments [7,8] and polymeric routes [9]. Sol–gel methods have been widely used for the preparation of nanocrystalline powders due to their low processing temperature, economic cost, and easy control of compositions. However, no reasearch is reported on transparent zirconia from sol–gel powders instead of commercial high purity powders [10–12]. In order to produce polycrystalline materials with high optical transmittance, it is mandatory to start with fine deagglomerated powders with chemical and phase purity and, very importantly, a narrow particle size distribution. It has been known that the nanopowders synthesized by wet-chemical methods are difficult to prepare transparent ceramics due to the formation of coarse agglomerates and the irregular shapes, which could be a common problem that reduces sinterability and homogeneity of the microstructure in the formed product [13]. Therefore, it is critical to obtain the cheap nanocrystalline powders for the transparent ceramics.

* Corresponding author at: State Key Lab of Advanced Technology for Materials Synthesis and Processing, Wuhan University of Technology, Wuhan 430070, China. Tel.: +86 027 87867862; fax: +86 027 87215421.
E-mail addresses: leiliwen@whut.edu.cn, leiliw@sohu.com (L. Lei).

0272-8842/$36.00 © 2011 Published by Elsevier Ltd and Techna Group S.r.l.
doi:10.1016/j.ceramint.2011.05.122

Spark plasma sintering (SPS) is a newly developed densification technique and has been successfully used for preparations of fully dense and fine-grained transparent ceramics. In a SPS process, the die and powders are directly heated b y pulsed electric current and its rapid heating and cooling rate can effectively suppress grain growth in final products. In the present study, a glycine-nitrate process combining high-energy ball milling was reported for the synthesis of highly sinterable 8YSZ nanopowder, from which transparent 8YSZ ceramics were prepared using SPS technique. The effects of calcination temperature on precursor powders and sintering process on optical property and microstructure were discussed as well.

2. Experimental procedure

2.1. Material preparation

The starting materials were $Zr(NO_3)_4{\cdot}5H_2O$ and $Y(NO_3)_3{\cdot}6H_2O$. These were mixed together according to the composition of 92 mol% ZrO_2 + 8 mol% Y_2O_3 and dissolved in deionized water. Then glycine was added as a fuel to the resulting solution. The molar ratio of glycine to total metal ions (Zr + Y) was 2.5:1. Precursors were prepared by adding ammonia to the mother solution at a rate of 3 mL/min with stirring to pH = 8. Afterwards, the solution was mixed with ethylene glycol (EG) to promote esterification reaction. The molar ratio of glycine:EG was 1:1. The obtained solution was heated on a hot plate at 75 °C with stirring to form gel precursors. After aging for 12 h, the gel was filtered and washed with ethanol for several times. Then the gel was dried at 150 °C and ignited to brown powders. In order to break the foamy agglomerates, two times planetary ball milling was adopted. The brown powders were firstly ball-milled with high-purity zirconia ball. The ball milling was carried out in isopropyl alcohol with 3 wt% polyethylene glycol addition for 12 h at rotational speed of 200 rpm. The mixture after ball milling was dispersed by supersonic vibration for 30 min and dried in a rotary evaporator. Then the powder was further calcined at different temperatures for 2 h. Finally, the calcined powders were ball-milled again with zirconia ball for 12 h in isopropyl alcohol again. After dried by rotary evaporator, the powder was consolidated by spark plasma sintering technique. SPS sintering was performed in a Dr. Sinter 1050 (Sumitomo Coal Mining Co., Japan) apparatus. The powder was loaded into a graphite die with an inner diameter of 15 mm with 50 MPa unixial pressure. The temperature was automatically increased to 600 °C within 10 min, from where and onwards the pressure was increased to 100 MPa and a heating rate of 100 °C/min was applied. The specimens were sintered at 1200–1350 °C for 5 min.

2.2. Characterizations of specimens

The thermal analysis of the precursor was conducted using thermogravimetric/differential thermal analysis (TG/DSC, Model STA449F3, Netzsch, Germany) in air at a heating rate of 10 °C/min. Phase identification was conducted using X-ray diffractometry (XRD) (Ultima, Rigaku, Japan) using CuKα radiation. The measurements were conducted at room temperature in 25–95° at a scanning rate of 6°/min. The microstructures of the powders and the sintered specimens were characterized using scanning electron microscope (SEM, Hitachi-S3400N) and transmission electron microscope (TEM, CM12/STEM, Philips). The in-line transmittance was measured in the wavelength range of 200–800 nm using a spectrophotometer (UV2550, Shimadzu).

3. Results and discussion

TG/DSC curves of the precursor are shown in Fig. 1. The total weight loss is 11.74 wt% up to 1000 °C. One endothermic and two exothermic peaks are observed as well. The endothermic peak centered at 133.5 °C is mainly due to the evaporation of adsorbed water and the release of molecular water. The exothermic peaks located at 403.1 °C and 695.2 °C are caused by the decomposition and oxidation of NO^{3-} and the crystallization of YSZ powder, respectively.

XRD patterns of the precursor and the powders calcined at different temperatures for 2 h are shown in Fig. 2. The results reveal that initial precursor is amorphous. The specimen calcined at 600 °C shows low crystallinity. After calcined at 700 °C, the precursor is completely decomposed and well crystallized. All the peaks of the powders calcined above 700 °C can be indexed by cubic YSZ (PDF: 30-1468). Futhermore, the crystallization temperature of YSZ found by XRD is slightly lower than that by DSC (Fig. 1), which could be due to the temperature hysteresis in the DSC measurement [14]. It could be also found that the peaks become sharper with the increase of the calcination temperature, which is attributed to grain growth.

The original precursors are foamy structure with the size of 10 μm as shown in Fig. 3(a). This large foamy structure could be broken in smaller fragments by planetary ball milling. The fragments begin to decompose into the spherical particles with the increase of calcination temperature. When the calcined temperature increased to 900 °C, the mean particle size is around 50 nm. It is well known that the high energy ball milling is an effective method to break the agglomeration [15,16]. However, the shape of the products by ball milling is not often uniform, which would induce the microstructure heterogeneities and limit the final density after high-temperature sintering. In addition, the crystallinity and the original structure will be partly destroyed by ball milling, which is detrimental to the densification in the sintering process. Furthermore, the foamy structure of the precursor was very porous and may lead to the bulk shape and hard agglomeration. The breaking of foamy structure is beneficial to form the spherical shape and reduce the possibility of agglomeration. Therefore, the precursor is ball-milled before calcining to final powder. Moreover, the powder may agglomerate during the calcining process again. Hence, the second ball milling is adopted to break the agglomeration further.

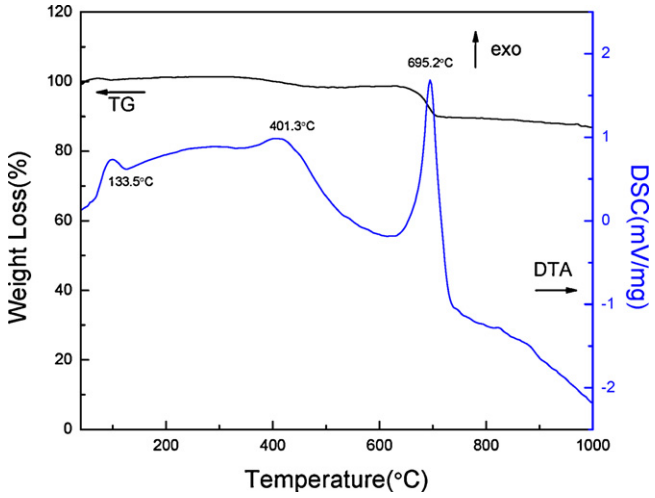

Fig. 1. DSC/TG curvers of the perescursor.

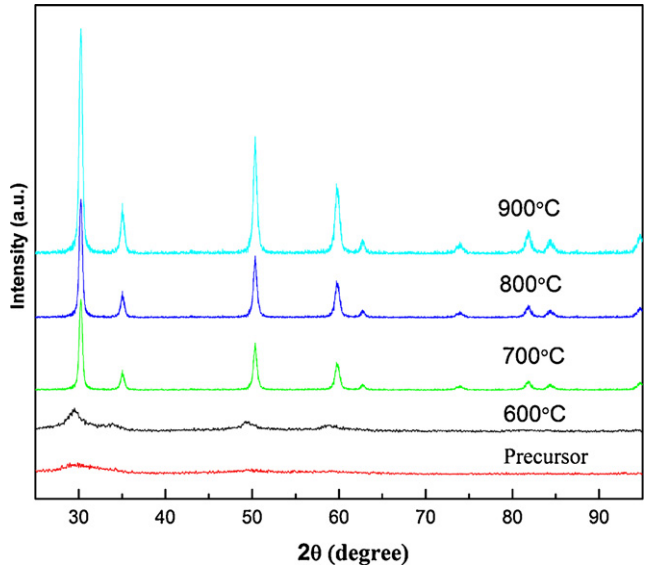

Fig. 2. X-ray diffraction profiles of the precuresors before and after calcining at different temperature.

To evaluate the effect of the calcination temperature on the sintering activity of final powders, the powders calcined at 700 and 900 °C were pressed into pellets and followed by annealing at 1100 °C for 1 h in the muffle furnace. The pellet from the powder calcined at 700 °C is still powder-like without obvious sign of sintering while the pellet made from the powder calcined at 900 °C was densified into porous ceramics with apparent grain growth as shown in Fig. 4(b). Qin et al. reported that the particles obtained at low calcination temperature were porous, which would cause nonuniform compaction and porosity [14]. These microstructure inhomogeneities limit the powder compact to achieve high final density after high-temperature sintering. Furthermore, the nanoparticles calcined at higher temperature have clearer profile and higher purity than those obtained from lower temperature calcination, which is beneficial to following densification process. However, higher calcination temperature would lead to the consumption of specific surface area of nanopowders and decrease sinterability, which is detrimental to sintering. Therefore, the favorable calcination temperature in present case was 900 °C for obtaining fine 8YSZ nanopowders with good dispersion and high sinterability.

Microstructural evolutions of 8YSZ ceramics sintered at elevating temperatures are shown in Fig. 5. For the specimens sintered at 1200 and 1250 °C, grain size was still suppressed in nanometric range. No extensive grain growth occurred and pores were mainly distributed at grain boundaries. During early and intermediate stage of SPS process, grain creeping and sliding is the dominating mechanism for densification, which is helpful to break hard agglomerates and large pores and involves no grain growth. With sintering temperature increasing, grain size was observed blooming into micrometers at temperature above 1250 °C. With the increasing in grain size and density, further densification by grain sliding is much difficult and will be dominated by grain-boundary diffusion. Grain growth of 8YSZ is oxygen vacancy dependent. At higher temperature, the diffusion rate of oxygen vacancy is greatly enhanced. As a result, pores would be entrapped by fast grain-boundary migration, which resulted in the pore distribution from intergranular to intragranular.

The light transmission of polycrystalline ceramics is sensitive to several microstructural factors, such as grain boundary, second phase, impurities, and residual pores. These factors act as a source of light scattering and absorption losses due to the difference of refractive index [17,18]. The porosity was measured by the combination of the Archimedes method and the counting method from SEM pictures because the former is insensitive to extremely low porosity. Pore size and the porosity in the specimens sintered by SPS at different temperatures are shown in Table 1. The specimens sintered at 1200 °C and 1250 °C are opaque due to high porosity. From

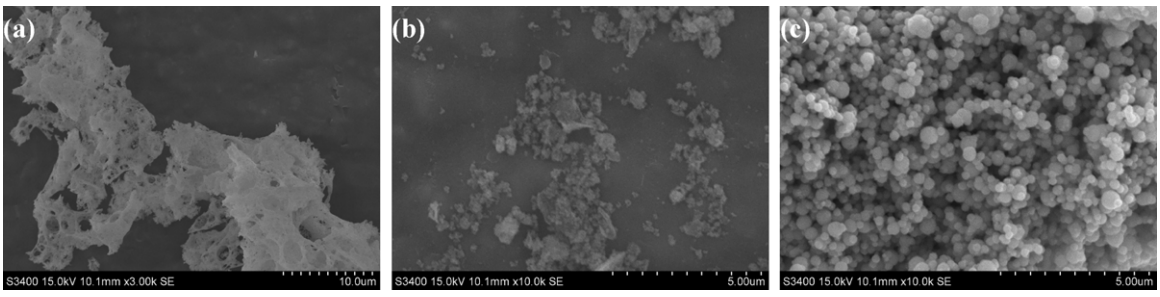

Fig. 3. SEM images of (a) the precursor, (b) the precursor after ball milling and (c) the powder calcined at 900 °C.

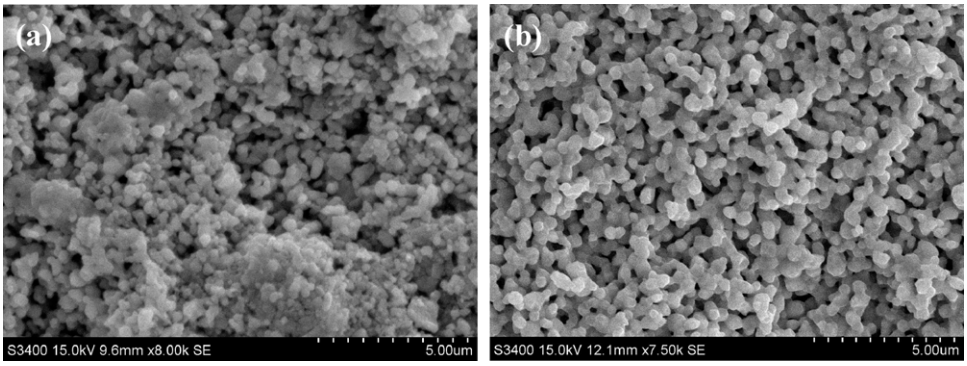

Fig. 4. SEM images of the specimens calcined in air at (a) 700 °C and (b) 900 °C.

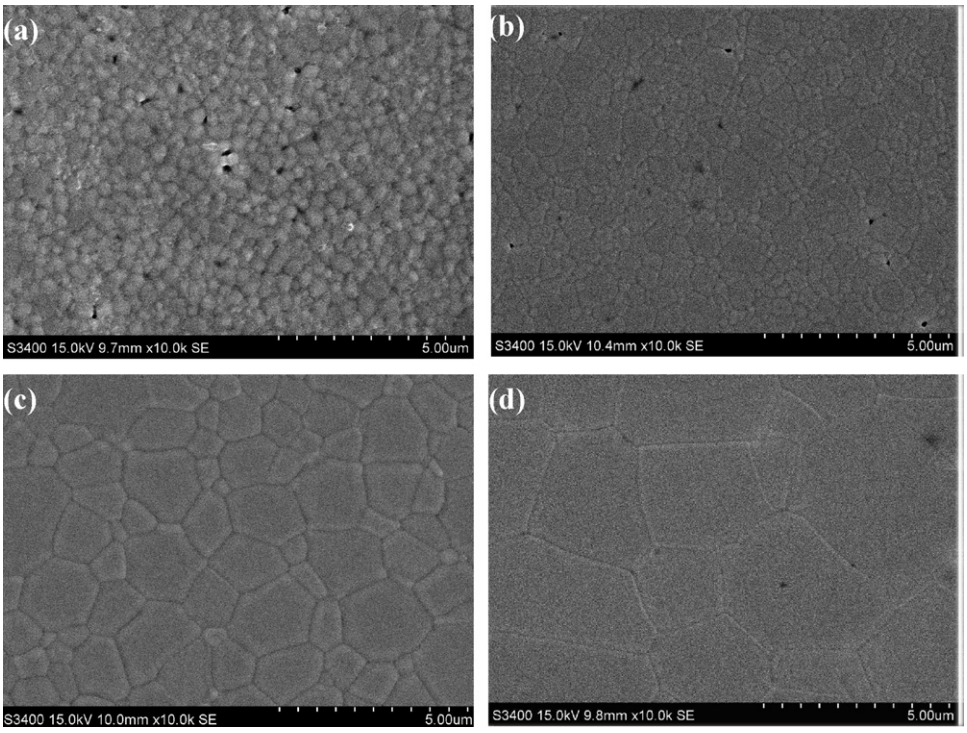

Fig. 5. SEM micrographs from the thermally etched surfaces of the samples sintered by SPS at different temperatures: (a) 1200 °C, (b)1250 °C, (c) 1300 °C and (d)1350 °C.

Table 1, the porosity of the specimens sintered at 1300 °C and 1350 °C is less than 0.1%. On the basis of the Mie theory, the effect of residual pore on the in-line transmittance can be written as:

$$T = (1 - R)^2 \exp(-C_{\text{sca}} t)$$

Table 1
Pore size and the porosity in 8YSZ samples sintered by SPS at different temperatures.

Sintering temperature (°C)	Porosity (%)	Average pore size (nm)	The largest pore size (nm)
1200	>0.1	280	300
1250	>0.1	120	250
1300	8.5×10^{-4}	60	240
1350	8.6×10^{-3}	120	500

where R is the reflection loss at two specimen surfaces, C_{sca} is the total scattering coefficient and t is the specimen thickness. For detailed calculations see Ref. [19]. The results of calculated and experimental value are presented in Fig. 6. As shown, the in-line transmittance is greatly dependent on the porosity. Meanwhile, the experimental data show an abrupt decline around 300 nm, which was attributed to the band gap of zirconia at 295 nm. The decline would correspond to the absorption edge [4]. The calculated data fit well with the experimental value for the specimen sintered at 1300 °C, while the inconsistence is found for the specimen sintered at 1350 °C above 600 nm range. One of the possible reasons for the deterioration of the transmittance may be related to the grain boundary scattering. For the isotropic cubic crystal structure, light scattering by grain boundary would be neglected due to the absence of the birefringence-induced light scattering at the grain boundary and the narrow grain boundary (always 1 nm

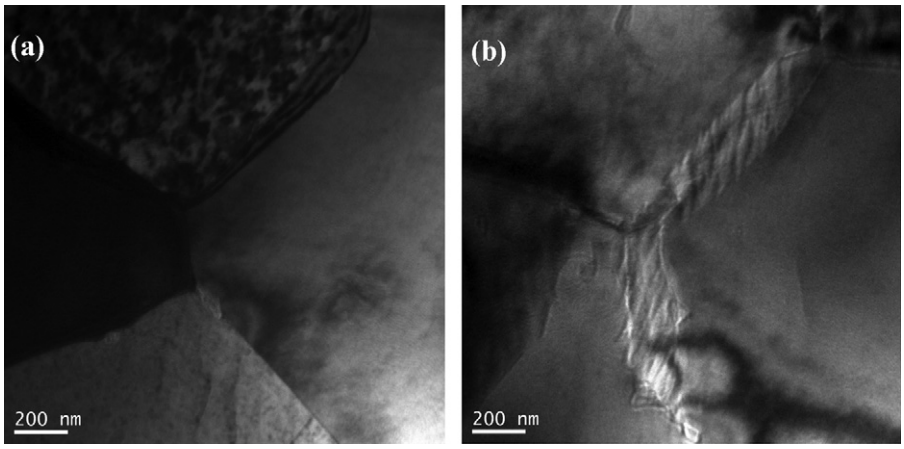

Fig. 7. TEM image of the samples sintered at different temperatures: (a) 1300 °C and (b)1350 °C.

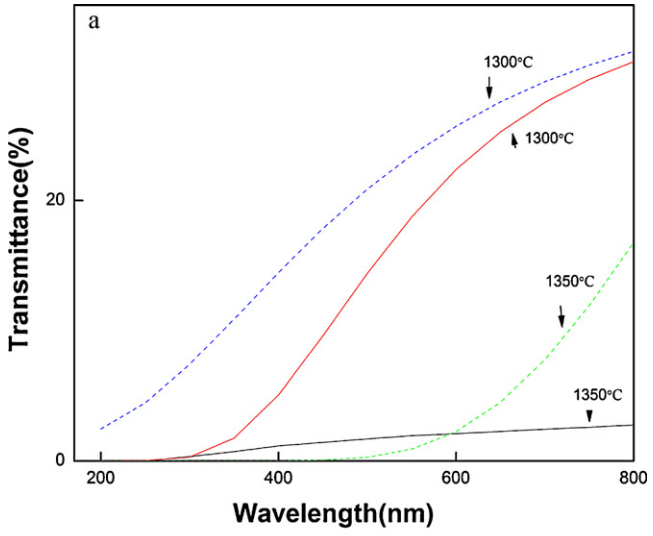

Fig. 6. (a) In-line transmittance dependent on sintering temperature. The dashed lines refer to the experimental value and the solid lines refer to the calculated data. (b) The optical transparency of the 0.6 mm thick disc fabricated at 1300 °C.

and far smaller than the wavelength of light). However, as shown Fig. 7, some grain boundaries of the specimen sintered at 1350 °C are far wider than 1 nm and much broader than these of the specimen sintered at 1300 °C. This may be attributed to the high temperature. In some instances, increasing the temperature allows more di- and trivalent segregated at the grain boundary, which can induce the glass phase enrichment and broaden the grain boundary [20]. In present case, the scattering of grain boundary cannot be neglected because of the broadened grain boundary. Another possible reason could be correlated to the oxygen vacancy, generated by the reducing conditions during SPS sintering. More oxygen vacancies would create accompanied with increasing temperature. According to the explanation by Savoini and Umberto [2,21], the vacancies present in large concentrations could coalesce at high temperatures and develope into cavities due to carbothermal reduction condition during the SPS processing. Alaniz et al. [11] reported that the transmittance could be tailored by post-processing annealing and the oxygen vacancies associated with a free electron could be annealed out in air. However, the cavities formed at higher sintering temperature could hardly be eliminated by annealing in air, which would cause great light scattering.

4. Conclusion

Highly sinterable nanometric 8YSZ powder was synthesized using the combination of glycine-nitrate process and high-energy ball milling. Appropriate planetary ball-milling could effectively break agglomerates to get homogenous nanopowder. Effect of the calcination temperature on the sintering activity of the powders was discussed. The 8YSZ nanopowder obtained from 900 °C calcination was 50 nm in spherical shape with good sinterability. Using the nanocrystalline powders, 8YSZ ceramics were prepared by SPS at 1200 and 1350 °C for 5 min. For the specimens sintered at 1200 °C and 1250 °C, many large pores are observed at the grain boundary. With the increasing of the sintering temperature, the grain grows while the porosity and pore size decreases distinctly. Extensive grain growth was observed at 1300 °C. As a result, pores tend to separate from the grain boundaries and become intragranular pores. Transparent 8YSZ ceramics were prepared by SPS sintering at 1300 °C for 5 min. The calculated data based on Mie theory are in agreement with the experimental value for the specimen sintered at 1300 °C, while the two data are inconsistent for the specimen sintered at 1350 °C above 600 nm. The reason for this may be attributed to the scattering by grain boundaries and higher oxygen vacancies.

Acknowledgement

This research was financially supported by National Natural Science Fondation of China (A3 Foresight Program-50821140308).

References

[1] U. Peuchert, Y. Okano, et al., Transparent cubic-ZrO_2 ceramics for application as optical lense, J. Eur. Ceram. Soc. 29 (2009) 283–291.
[2] U. Anselmi-Tamburini, J.N. Woolman, Z.A. Munir, Transparent nanometric cubic and tetragonal zirconia obtained by high-pressure pulsed electric current sintering, Adv. Funct. Mater. 17 (2007) 3267–3273.
[3] A. Krell, J. Klimke, T. Hutzler, Transparent compact ceramics: inherent physics issues, Opt. Mater. 31 (2009) 1144–1155.
[4] K. Tsukuma, I. Yamashita, Transparent 8 mol% Y_2O_3–ZrO_2(8Y) ceramics, J. Am. Ceram. Soc. 91 (2008) 813–818.
[5] J. Fenech, C. Viazzi, J.-P. Bonin, F. Ansart, A. Barnabe, Morphology and structure of YSZ powders: comparison between xerogel and aerogel, Ceram. Int. 35 (2009) 3427–3433.
[6] J. Judes, V. Kamaraj, Sol–gel preparation and characterization of ceria stabilized zirconia minispheres, J. Sol–Gel Sci. Technol. 49 (2009) 159–165.
[7] G. Dell'Agli, G. Mascolo, Zirconia–yttria (8 mol%) powders hydrothermally synthesized from different Y-based precursors, J. Eur. Ceram. Soc. 24 (2004) 915–918.
[8] X. Xin, Z. Lu, X. Huang, X. Sha, Y. Zhang, W. Su, Influence of synthesis routes on the performance from weakly agglomerated yttria-stabilized zirconia nanomaterials, Mater. Res. Bull. 41 (2006) 1319–1329.
[9] S. Farhikhteh, A. Maghsoudipour, B. Raissi, Synthesis of nanocrystalline YSZ (ZrO_2–$8Y_2O_3$) powder by polymerized complex method, J. Alloys Compd. 491 (2010) 402–405.
[10] S.R. Casolco, J. Xu, J.E. Garay, Transparent/translucent polycrystalline nanostructured yttria stabilized zirconia with varying colors, Scripta Mater. 58 (2008) 516–519.
[11] J.E. Alaniz, F.G. Perez-Gutierrez, G. Aguilar, J.E. Garay, Optical properties of transparent nanocrystalline yttria stabilized zirconia, Opt. Mater. 32 (2009) 62–68.
[12] S. Ghosh, D. Teweldebrhan, J.R. Morales, J.E. Garay, et al., Thermal properties of the optically transparent pore-free nanostructured yttria-stabilized zirconia, J. Appl. Phys. 106 (2009) 113507.
[13] M. Trunec, K. Maca, Compaction and pressureless sintering of zirconia nanoparticles, J. Am. Ceram. Soc. 90 (2007) 2735–2740.
[14] Xiapeng, Qin, H. Yang, G. Zhou, et al., Synthesis of submicron-sized spherical Y_2O_3 powder for transparent YAG ceramics, Mater. Res. Bull. 46 (2011) 170–174.
[15] Y. Huang, D. Jiang, J. Zhang, Precipitation synthesis and sintering of lanthanum doped yttria transparent ceramics, Opt. Mater. 31 (2009) 1448–1453.
[16] H. Huang, H. Gong, D. Tang, O.K. Tan, Synthesis and characterization of yttrium aluminum garnet by high-energy ball milling, Opt. Mater. 31 (2009) 716–719.
[17] R. Chaim, M. Kalina, et al., Transparent yttrium aluminum garnet (YAG) ceramics by spark plasma sintering, J. Eur. Ceram. Soc. 27 (2007) 3331–3337.
[18] B.-N. Kim, K. Hiraga, Koji, H. Yoshida, Spark plasma sintering of transparent alumina, Scripta Mater. 57 (2007) 607–610.
[19] J.G.J. Peelen, R. Metselaar, Light scattering by pores in polycrystalline materials: transmission properties of alumina, J. Appl. Phys. 45 (1974), 246-220.
[20] X. Guo, Physical origin of the intrinsic grain-boundary resistivity of stabilized-zirconia: role of the space-charge layers, Solid State Ionics 99 (1997) 235–242.
[21] B. Savoini, C. Ballesteros, J.E. Munoz Santiuste, R. Gonzalez, Y. Chen., Thermochemical reduction of yttria-stabilized-zirconia crystals: optical and electron microscopy, Phys. Rev. B 57 (1998) 13439–13447.